Perylene-Derived Single-Component Organic Nanoparticles with Tunable Emission: Efficient Anticancer Drug Carriers with Real-Time Monitoring of Drug Release

Avijit Jana,[†] Kim Truc Nguyen,[†] Xin Li,[‡] Pengcheng Zhu,[§] Nguan Soon Tan,[§] Hans Ågren,[‡,*] and Yanli Zhao[†,⊥,*]

[†]Division of Chemistry and Biological Chemistry, School of Physical and Mathematical Sciences, Nanyang Technological University, 21 Nanyang Link, Singapore 637371, [‡]Department of Theoretical Chemistry and Biology, School of Biotechnology, KTH Royal Institute of Technology, Stockholm, Sweden SE-10691, [§]School of Biological Sciences, Nanyang Technological University, 60 Nanyang Drive, Singapore 637551, and [⊥]School of Materials Science and Engineering, Nanyang Technological University, Singapore 639798

ABSTRACT An organic nanoparticle-based drug delivery system with high drug loading efficacy (~79 wt %) was developed using a perylene-derived photoremovable protecting group, namely, perylene-3,4,9,10-tetrayltetramethanol ($Pe(OH)_4$). The anticancer drug chlorambucil was protected by coupling with $Pe(OH)_4$ to form photocaged nanoparticles ($Pe(Cbl)_4$). The photorelease mechanism of chlorambucil from the $Pe(Cbl)_4$ conjugate was investigated experimentally by high-resolution mass spectrometry and theoretically by density functional theory calculations. The $Pe(Cbl)_4$ nanoparticles perform four important roles: (i) a nanocarrier for drug delivery, (ii) a phototrigger for drug release, (iii) a fluorescent chromophore for cell imaging, and (iv) a photoswitchable fluorophore for real-time monitoring of drug release. Tunable emission of the perylene-derived nanoparticles was demonstrated by comparing the emission properties of the $Pe(OH)_4$ and $Pe(Cbl)_4$ nanoparticles with perylene-3-ylmethanol. These nanoparticles were subsequently employed in cell imaging for investigating their intracellular localization. Furthermore, the *in vivo* toxicity of the $Pe(OH)_4$ nanoparticles was investigated using the mouse model. Histological tissue analysis of five major organs, *i.e.*, heart, kidney, spleen, liver, and lung, indicates that the nanoparticles did not show any obvious damage to these major organs under the experimental conditions. The current research presents a successful example of integrating multiple functions into single-component organic nanoparticles for drug delivery.

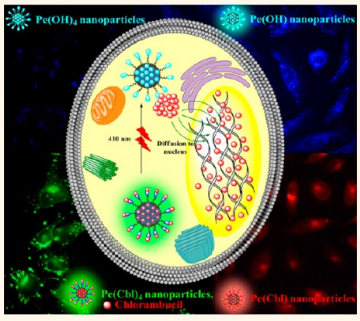

KEYWORDS: chlorambucil · drug delivery · organic nanoparticles · photoremovable protecting group · tunable emission

In order to enhance therapeutic efficacy, the protection of drug molecules from leaching, degradation, or interaction with the biological environment before reaching the target sites is crucial for drug delivery systems (DDSs).[1] In recent years, many sophisticated stimuli-responsive DDSs based on metallic nanoparticles,[2−6] ceramic nanoparticles,[7−11] polymers,[12,13] dendrimers,[14−16] liposomes,[17−19] and micelles[20,21] have been developed. Though these nanocarriers have their own advantages such as easy synthesis, tunable particle size, and low cytotoxicity, they often suffer from several serious limitations including (i) premature release or leaching of loaded drug molecules, (ii) imprecise control of the drug release over an extended period of time, and (iii) low drug loading efficacy (*e.g.*, 2.5% for Au nanoparticles,[3] 0.9% for Fe_3O_4 nanoparticles,[4] 9.9% for hollow mesoporous silica nanoparticles,[11] and 6.0% of doxorubicin for mesoporous silica nanoparticles[22]), resulting in the utilization of a large amount of unwanted carriers.

Among various externally regulated stimuli, light is one of the best agents for triggering the release of drugs from the above-mentioned DDSs since the activation processes by light are rapid and clean and allow for low invasiveness as far as biological systems are concerned. Thus, light-induced

* Address correspondence to zhaoyanli@ntu.edu.sg; agren@theochem.kth.se.

Received for review February 23, 2014 and accepted May 13, 2014.

Published online May 13, 2014
10.1021/nn501073x

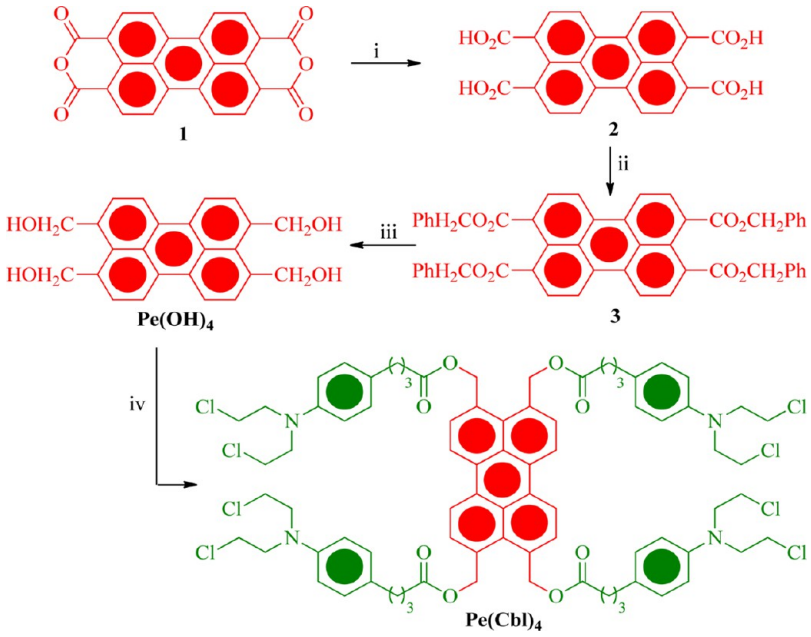

Scheme 1. Synthesis of photocaged prodrug $Pe(Cbl)_4$. Reagents and conditions: (i) KOH, H_2O, reflux, 24 h, (ii) $PhCH_2Cl$, K_2CO_3, DMAP, 18-crown-6, DMF, 90 °C, 24 h, (iii) DIBALH, DCM, −78 °C to room temperature, 48 h, and (iv) chlorambucil, EDCL, DMAP, DCM, room temperature, overnight.

drug release techniques have been applied frequently for spatially and temporally controlled release of bioactive molecules from DDSs both *in vitro*[23−26] and *in vivo*.[27,28] Light-induced drug release is usually achieved by irradiating a photocaged prodrug by means of either one-photon or two-photon irradiation.[29] Photocaging refers to temporary inactivation of a biologically active molecule using a photoremovable protecting group (PRPG).[30,31] In this process, since the drug molecule is covalently attached with a photoactive molecule, it loses its activity temporarily, thereby ruling out the possibility of premature release or leaching of the drug molecule. Once the system reaches the target site, the drug can be released from the photoactive molecule through photolysis, thus restoring its activity. To accomplish an optimal therapeutic efficacy, the real-time spatial and temporal tracking of DDSs within living cells is also important for drug delivery. Except for magnetic nanoparticle-based DDSs that can be tracked by magnetic resonance imaging (MRI) techniques, the above-mentioned DDSs are often nonfluorescent. Therefore, it is necessary to make them visually traceable by rigorous chemical modifications.

By keeping these considerations in mind, we herein report a successful development of a photoresponsive organic nanoparticle-based DDS with enhanced drug loading efficacy (~79 wt %). In this case, an anticancer drug, chlorambucil, was protected by coupling it with perylene-3,4,9,10-tetrayltetramethanol ($Pe(OH)_4$) as a PRPG in a 4:1 molar ratio to form a photocaged fluorescent ester conjugate ($Pe(Cbl)_4$). The organic nanoparticle-based DDS with tunable emission was then prepared from the $Pe(Cbl)_4$ conjugate for photoinduced chlorambucil delivery under real-time monitoring of drug release *in vitro*. The present DDS performs four important roles simultaneously: (i) a nanocarrier for drug delivery, (ii) a phototrigger for the drug release, (iii) a fluorescent chromophore for cell imaging, and (iv) a photoswitchable fluorophore for real-time monitoring of drug release.

RESULTS AND DISCUSSION

Synthesis and Characterization of $Pe(Cbl)_4$ Nanoparticles. To synthesize the photocaged prodrug $Pe(Cbl)_4$, commercially available perylene-3,4,9,10-tetracarboxylic dianhydride was employed to prepare perylene-3,4,9,10-tetrayltetramethanol ($Pe(OH)_4$) in three steps by following a literature procedure.[32] Finally, the caging of four equivalents of the anticancer drug chlorambucil with PRPG $Pe(OH)_4$ was achieved by carrying out EDCL (1-ethyl-3-(3-(dimethylamino)propyl)carbodiimide) coupling in the presence of 4-dimethylaminopyridine (DMAP) in dichloromethane (DCM) as depicted in Scheme 1.

After successful preparation of the photocaged $Pe(Cbl)_4$ conjugate, we proceeded to synthesize the $Pe(Cbl)_4$ nanoparticles for drug delivery by using a reprecipitation technique, *i.e.*, slowly adding a $Pe(Cbl)_4$ acetone solution (10 μL, 5 mM) into water (5 mL) with constant sonication for 30 min. By employing a similar reprecipitation technique, $Pe(OH)_4$-based nanoparticles were also synthesized as the control. The shape and morphology of the resulting $Pe(Cbl)_4$ and $Pe(OH)_4$ nanoparticles were determined by transmission electron microscopy (TEM) and scanning electron microscopy (SEM). It was

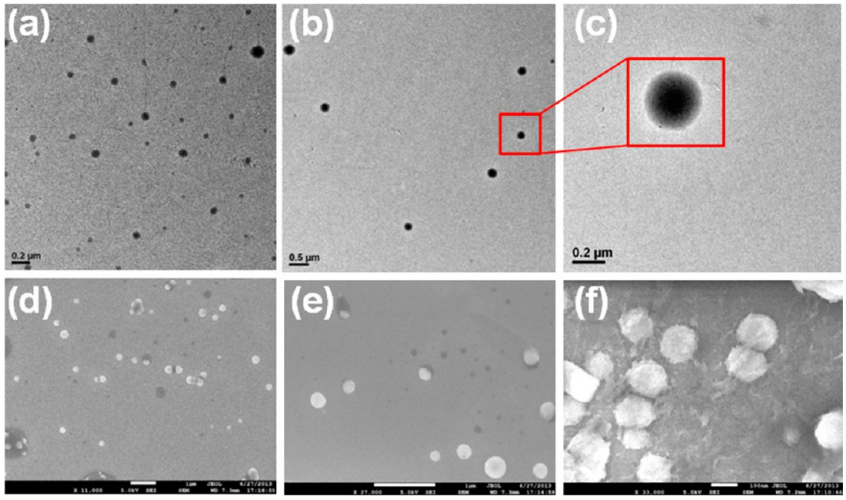

Figure 1. TEM images of (a) $Pe(OH)_4$ nanoparticles, (b) $Pe(CbI)_4$ nanoparticles, and (c) $Pe(CbI)_4$ nanoparticles with higher magnification. SEM images of (d) $Pe(OH)_4$ nanoparticles, (e) $Pe(CbI)_4$ nanoparticles, and (f) $Pe(CbI)_4$ nanoparticles with higher magnification. Scale bar = 1 μm (d, e) and 100 nm (f).

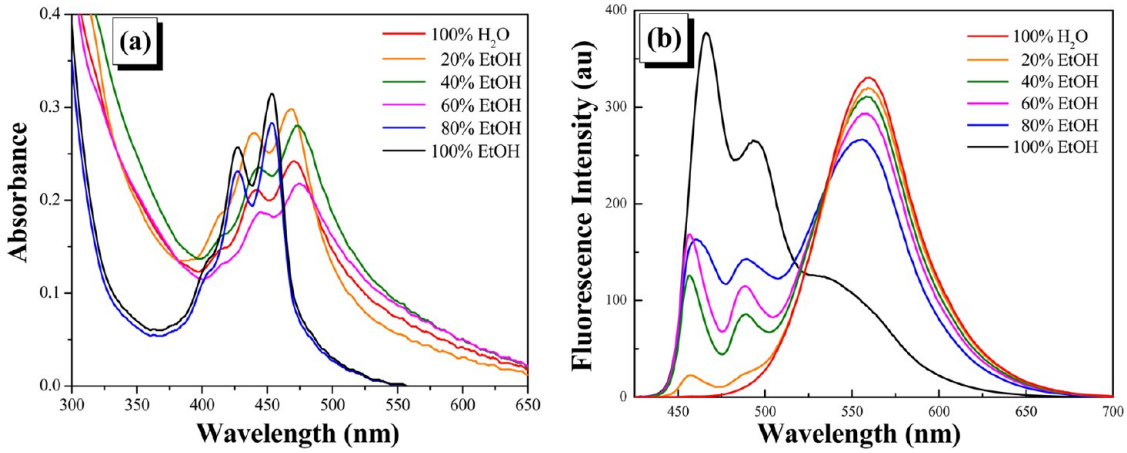

Figure 2. (a) UV−vis absorption and (b) emission spectra of photocaged conjugate $Pe(CbI)_4$ in water, ethanol, and aqueous ethanol.

found that both nanoparticles are spherical in shape (Figure 1). The size of the respective nanoparticles was measured by dynamic light scattering (DLS) analysis, and the average nanoparticle sizes were observed to be 220 and 175 nm, respectively (Figure S3 in the Supporting Information (SI)).

Photophysical Properties of $Pe(CbI)_4$. The UV−vis absorption and emission spectra of the photocaged prodrug $Pe(CbI)_4$ were recorded both in ethanolic solution and in aqueous suspension. The absorption spectrum of the caged prodrug in ethanolic solution was found to be quite similar to the spectrum of perylene, with strong absorption peaks centered at 405, 425, and 450 nm. Upon the addition of an increasing percentage of water, the absorption spectrum of $Pe(CbI)_4$ was slightly red-shifted as well as broadened, as shown in Figure 2a. The emission spectrum of $Pe(CbI)_4$ in ethanolic solution also resembles the emission spectrum of perylene with the emission peaks centered at 468, 490, and 525 nm. When adding an increasing percentage of water, the characteristic emission intensities of the perylene chromophore in $Pe(CbI)_4$ gradually decreased, while a new emission peak centered at 560 nm appeared with gradual enhancement of the emission intensity (Figure 2b). The appearance of the new emission peak at 560 nm can be ascribed to the formation of excimers[33] from the $Pe(CbI)_4$ nanoparticles.

Next, we examined the theoretical emission of the perylene dimer by optimizing the excited state of the dimer at the TD-PBE0/cc-pVDZ level of theory. According to a literature report,[33] this method is able to reasonably reproduce the emissive energy of aromatic excimers. The initial structure of the dimer was extracted from an MD (molecular dynamics) simulation trajectory. It was found that the highest occupied and lowest unoccupied molecular orbitals (HOMO and LUMO) of the dimer receive a sizable contribution from both perylene units (Figure 3), and the HOMO to LUMO transition exhibits charge transfer character from one

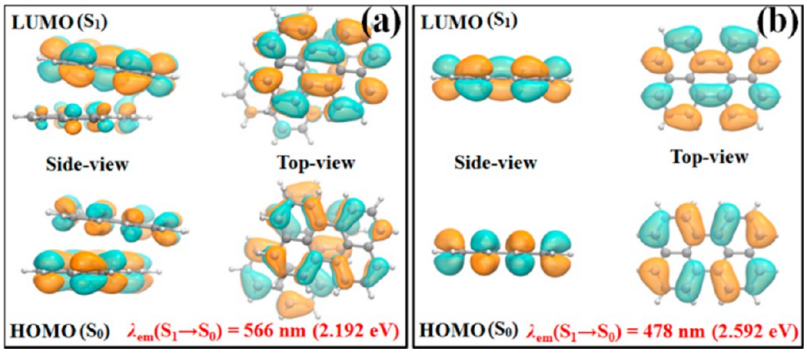

Figure 3. Frontier molecular orbitals and emissive energies of perylene: (a) dimer and (b) monomer. The geometry of the perylene dimer was extracted from the simulation trajectory and fed to time-dependent density functional theory (DFT) optimizations at the PBE0/cc-pVDZ level of theory to compute the emission energy.

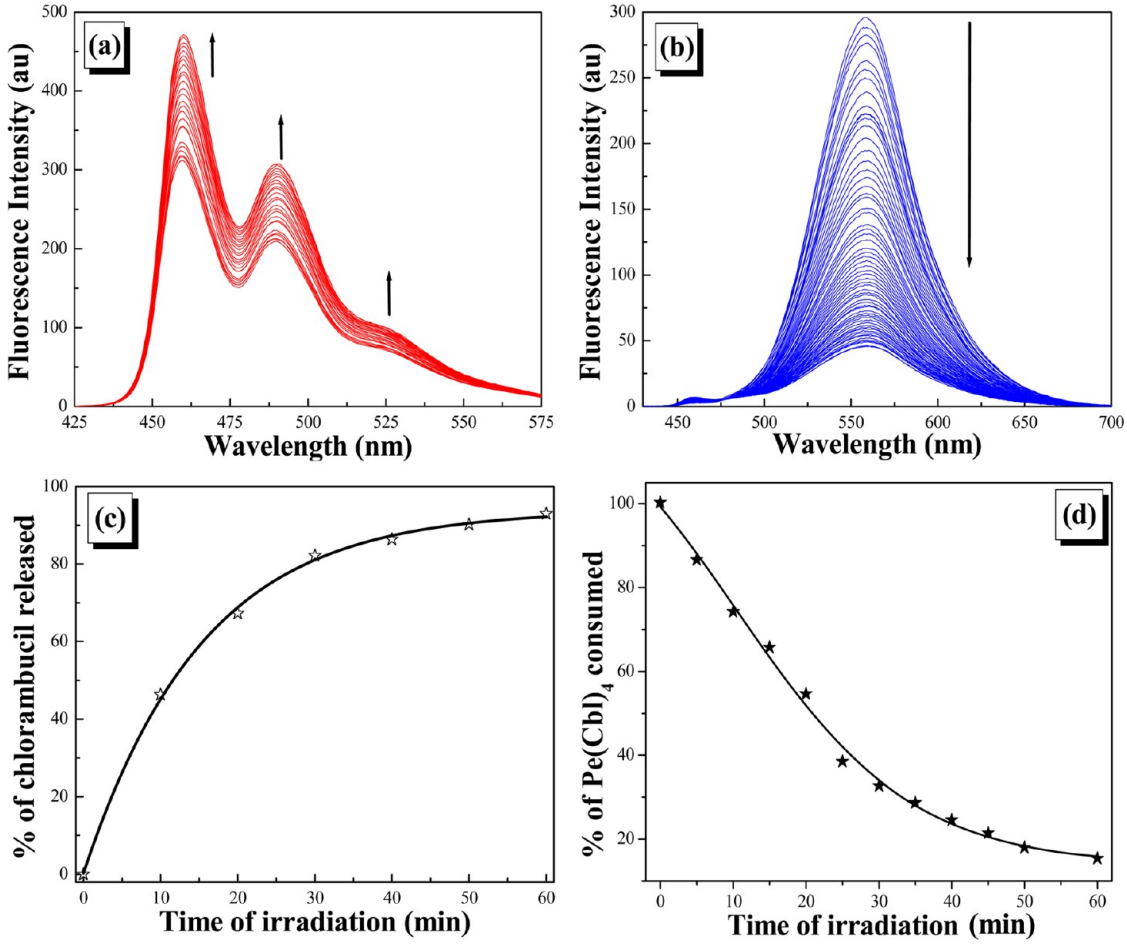

Figure 4. Emission spectra of the photocaged $Pe(CbI)_4$ conjugate in different time intervals of photoirradiation (0−60 min, ≥410 nm). Photolysis was carried out (a) in aqueous acetonitrile and (b) in aqueous suspension. (c) Percentage (%) of the drug released (normalized plot with a normalization factor of 4) and (d) percentage (%) of $Pe(CbI)_4$ decomposed in correlation with (b).

perylene to another. The vertical emissive energy of the excited state of the perylene dimer was obtained as 2.19 eV (566 nm), which shows a significant red shift as compared to that of the monomer (2.59 eV, 478 nm). The computed emissive energies for the perylene monomer and dimer are in fair agreement with experimental observations (Figure 2b), supporting the conclusion that the red-shifted emission arises from the aggregation of $Pe(CbI)_4$ and the formation of perylene dimers. Thus, the $Pe(CbI)_4$ nanoparticles we prepared could be expected to serve as a useful platform for live cell imaging as well as for intracellular tracking of nonfluorescent anticancer drug chlorambucil release.

Hydrolytic Stability of $Pe(CbI)_4$. To examine the hydrolytic stability of the $Pe(CbI)_4$ nanoparticles, phosphate-buffered saline (PBS) solutions (1 mL) containing

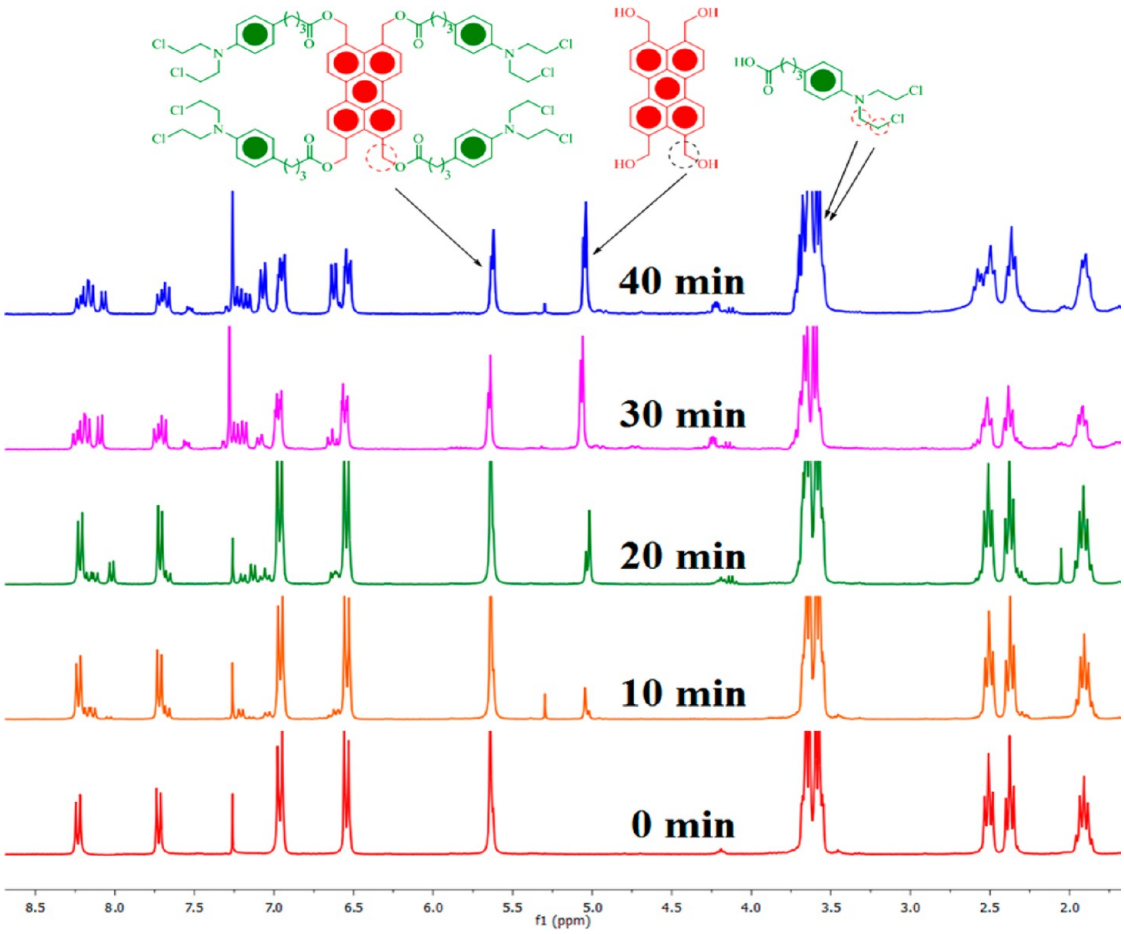

Figure 5. ^{1}H NMR spectral changes of Pe(Cbl)$_4$ at different irradiation times.

Pe(Cbl)$_4$ nanoparticles (2×10^{-4} M) at different initial pH values (5.6, 7.4, and 8) were prepared separately. PBS culture medium containing 10% fetal bovine serum (FBS) at pH 7.4 was also prepared to monitor the stability of the Pe(Cbl)$_4$ nanoparticles in the biological environment. All the tubes were kept in an ultrasonic bath for 10 min to make the solutions homogeneous and then stored at room temperature in the dark for 72 h. Next, the residue organic compounds were extracted in DCM, and ^{1}H NMR spectra were recorded to examine the remaining percentage of the Pe(Cbl)$_4$ molecule. Insignificant decomposition (4−6%) of the Pe(Cbl)$_4$ nanoparticles under the dark condition was observed (Table S1 in the SI), which proves that the Pe(Cbl)$_4$ nanoparticles are quite stable under the dark condition.

Photolysis of Photocaged Prodrug Pe(Cbl)$_4$. To demonstrate the photoinduced release of the anticancer drug chlorambucil, an aqueous acetonitrile solution of Pe(Cbl)$_4$ was irradiated under visible light (≥410 nm) by a 125 W (110 mW/cm^2) medium-pressure Hg lamp using a 1 M $NaNO_2$ solution as the UV filter. The course of the photorelease was followed by emission spectroscopy (Figure 4a) as well as by ^{1}H NMR spectroscopy. During the photolysis, the emission intensity of Pe(Cbl)$_4$ steadily increased, which is consistent with previously reported perylene-based PRPG.[1]

After successful demonstration of the photorelease of chlorambucil in solution, we carried out the photolysis of Pe(Cbl)$_4$ nanoparticles in aqueous suspension to prove that it is an efficient drug delivery vehicle. An aqueous suspension of the Pe(Cbl)$_4$ nanoparticles (1×10^{-4} M) was irradiated by following the same procedure as adopted in the case of the aqueous acetonitrile solution, and the course of photolysis was monitored by ^{1}H NMR spectroscopy (Figure 5). A known amount of aqueous suspension (5 mL) underwent photolysis at different irradiation times and was extracted in DCM followed by recording its ^{1}H NMR spectrum. A photocleavage process of Pe(Cbl)$_4$ nanoparticles into corresponding chlorambucil photoproduct along with other photoproducts was observed.

We also followed the photolysis process by emission spectroscopy (Figure 4b), which showed that, upon gradual photolysis, the emission intensity of Pe(Cbl)$_4$ nanoparticles gradually decreased, confirming the photodecomposition of Pe(Cbl)$_4$ nanoparticles. By correlating the decrease in the fluorescence intensity with the percentage of the drug released as well as

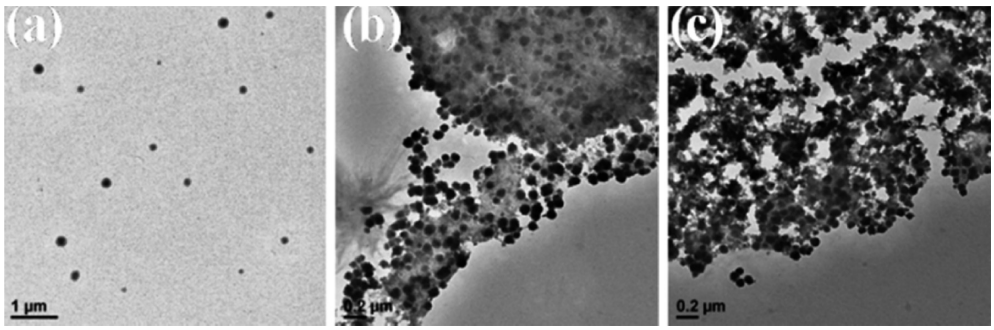

Figure 6. TEM images of $Pe(CbI)_4$ nanoparticles (a) before the photolysis, (b) after 20 min of photolysis, and (c) after 40 min of photolysis.

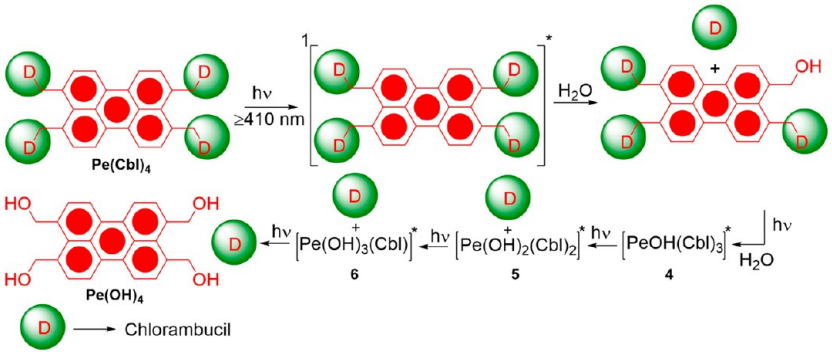

Scheme 2. Photorelease mechanism of chlorambucil.

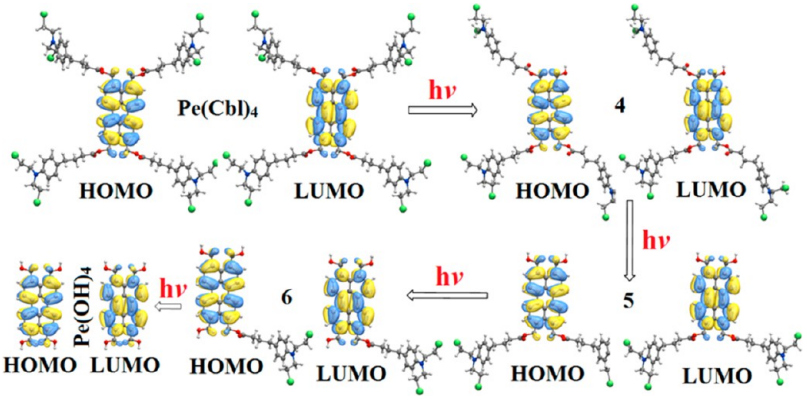

Figure 7. Contour plots of frontier molecular orbitals of $Pe(OH)_4$, $Pe(CbI)_4$, and compounds 4−6.

the percentage of $Pe(CbI)_4$ nanoparticles decomposed, it was noted that, after 60 min of photoirradiation, about 95% of drug was released as shown in Figure 4c. Furthermore, the fate of the $Pe(CbI)_4$ nanoparticles after the photolysis was investigated by TEM, which showed that, on gradual photolysis, the monodispersed spherical $Pe(CbI)_4$ nanoparticles gradually agglomerated with the loss of spherical morphology (Figure 6).

Proposed Mechanism for the Photorelease of Chlorambucil. On the basis of literature reports,[34,35] we proposed a stepwise pathway for the photorelease of chlorambucil from the photocaged $Pe(CbI)_4$ conjugate through an ionic mechanism. The initial photochemical step involves the excitation of the perylene-3,4,9,10-tetrayltetramethyl chromophore to its singlet excited state, which then undergoes heterolytic cleavage of one of the ester bonds to produce an ion-pair of a $[Pe(CbI)_3CH_2]^+$

TABLE 1. Computed Energy Levels of Frontier Molecular Orbitals of $Pe(OH)_4$, $Pe(CbI)_4$, and Compounds 4−6

compound	E_{HOMO} (eV)	E_{LUMO} (eV)	E_{gap} (eV)
$Pe(OH)_4$	−4.69	−1.72	2.97
$Pe(CbI)_4$	−5.20	−2.26	2.94
4	−5.07	−2.12	2.95
5	−4.94	−2.00	2.94
6	−4.82	−1.86	2.96

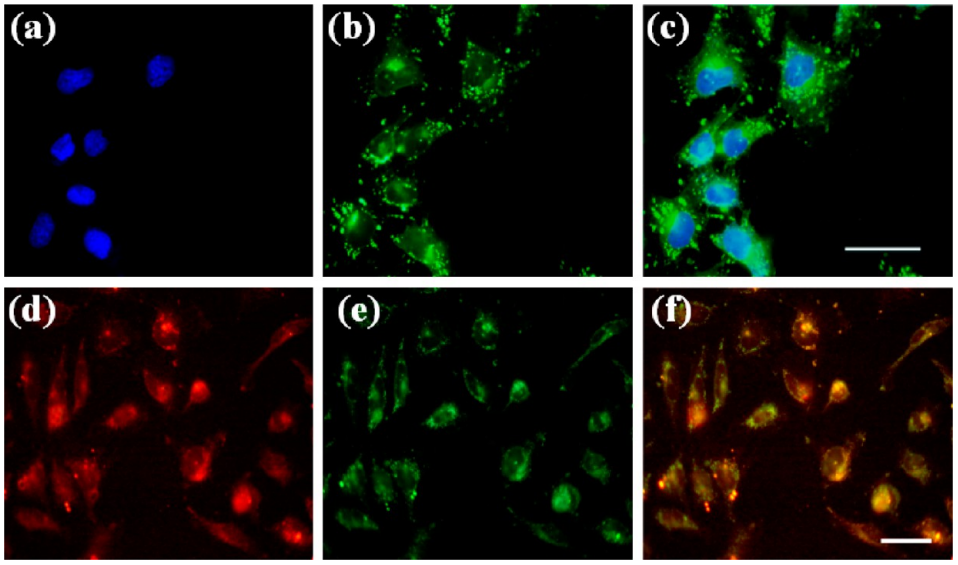

Figure 8. Intracellular trafficking studies of $Pe(Cbl)_4$ nanoparticles in HeLa cells: (a) emission from DAPI, (b) emission from $Pe(Cbl)_4$, and (c) overlay image of (a) and (b), scale bar = 50 μm. (d) Emission from LysoTracker Red DND-99, (e) emission from $Pe(Cbl)_4$, and (f) overlay image of (d) and (e), scale bar = 20 μm.

carbocation and a chlorambucil carboxylate anion. After the ion-pair separation in water, the methylenic carbocation and carboxylate anion react with water to yield the corresponding alcohol [$Pe(Cbl)_3CH_2OH$] and chlorambucil. The process continues until it releases four equivalents of chlorambucil with the production of the final byproduct $Pe(OH)_4$ as shown in Scheme 2. The above proposed mechanism was further supported by high-resolution mass spectrometry (HRMS) analysis of the $Pe(Cbl)_4$ nanoparticles after 20 min of photoirradiation. After the photoirradiation, the reaction mixture was subjected to HRMS analysis, and it was found that all the possible intermediates for the stepwise mechanism were present in the reaction mixture along with released chlorambucil (see pages S7, S8 in the SI).

Furthermore, the photorelease of four equivalents of chlorambucil from the $Pe(Cbl)_4$ nanoparticles was validated by DFT calculations. The geometries of $Pe(OH)_4$ and $Pe(Cbl)_4$ along with compounds **4**–**6** were optimized by DFT calculations with the B3LYP functional[36,37] implemented in the ORCA program.[38] From the computed frontier molecular orbitals shown in Figure 7, it can be seen that the HOMO and LUMO reside exclusively on the perylene core. The energy levels of HOMO and LUMO are influenced by the photolysis of the ester units. However, the HOMO–LUMO gap remains almost unchanged for all the above compounds, as shown in Table 1. Ground-state DFT calculations show that the products of photolysis are thermally more stable than their corresponding reactants by ~12 kJ mol^{-1} (Figure S6 and Table S2 in the SI), which suggest spontaneous photorelease of chlorambucil from the $Pe(Cbl)_4$ conjugate under photoirradiation.

Cellular Uptake and Intracellular Trafficking Studies of $Pe(Cbl)_4$ Nanoparticles. Real-time cellular uptake of $Pe(Cbl)_4$ nanoparticles was investigated by cell imaging using the HeLa cancer cell line. The HeLa cell line was maintained in minimum essential medium containing 10% FBS under humified conditions at 37 °C and 5% CO_2. HeLa cells (5×10^4 cells/well) were plated on six-well plates and allowed to adhere for 4–8 h. The cells were then incubated with $Pe(Cbl)_4$ nanoparticles (5×10^{-6} M) in cell culture medium at 37 °C and 5% CO_2 for 6 h. Thereafter, the cells were fixed in 4% aqueous formaldehyde solution for 15 min and washed two times with PBS. Imaging was acquired by a confocal microscope using respective filters. Cellular uptake after 6 h incubation reveals that the $Pe(Cbl)_4$ nanoparticles were readily internalized by the cells (Figure S7 in the SI).

In order to explore the intracellular localization of the $Pe(Cbl)_4$ nanoparticles inside HeLa cells, the cell nuclei and lysosome were stained with 4′,6-diamidino-2-phenylindole (DAPI) and LysoTracker Red DND-99, respectively. After exposing HeLa cells to $Pe(Cbl)_4$ nanoparticles for 6 h followed by fixation and subsequent staining with DAPI, confocal fluorescence microscopy studies reveal that the $Pe(Cbl)_4$ nanoparticles were readily internalized by the cells and mostly located in the cytoplasm (Figure 8a–c). By using a similar incubation procedure with $Pe(Cbl)_4$ nanoparticles for 6 h followed by staining with LysoTracker Red dye DND-99, the obtained images show that the $Pe(Cbl)_4$ nanoparticles were located both in the cytoplasm (Figure 8f, green color) and in the lysosome (Figure 8f, yellow color by the co-localization of $Pe(Cbl)_4$ nanoparticles and DND-99).

Anticancer Efficacy of $Pe(Cbl)_4$ Nanoparticles before and after Photolysis. After successful demonstration of the pronounced internalization of $Pe(Cbl)_4$ nanoparticles

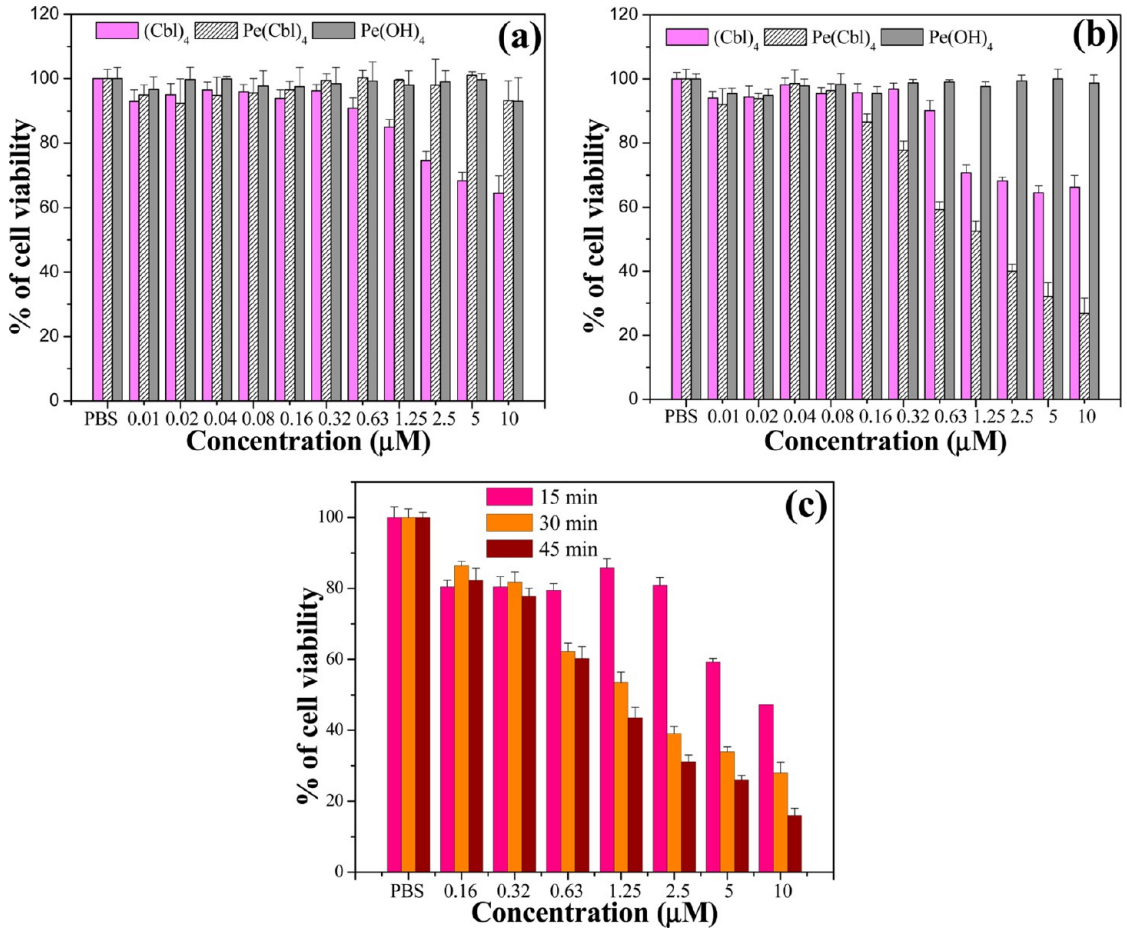

Figure 9. (a and b) Cell viability of HeLa cells incubated with $Pe(Cbl)_4$ nanoparticles, $Pe(OH)_4$ nanoparticles, and chlorambucil, respectively: (a) before irradiation and (b) after 30 min of irradiation. (c) Cell viability in the presence of different concentrations of $Pe(Cbl)_4$ nanoparticles at different time intervals of irradiation. Values are presented as mean ± SD.

by the cells, the *in vitro* cytotoxicity of $Pe(Cbl)_4$ nanoparticles, chlorambucil, and $Pe(OH)_4$ nanoparticles was evaluated using the MTT (3-(4,5-dimethylthiazol-2-yl)-2,5-diphenyltetrazolium bromide) assay on the HeLa cell line. Briefly, HeLa cells in their exponential growth phase were trypsinized and seeded into 96-well cell culture plates at a density of 1×10^4 cells/mL in 100 μL of DMEM (Dulbecco's modified Eagle medium) complete medium. Different concentrations of $Pe(Cbl)_4$ nanoparticles, chlorambucil (four equivalents with respect to each concentration of $Pe(Cbl)_4$ nanoparticles), and $Pe(OH)_4$ nanoparticles were added in the wells with an equal volume of PBS in the control wells. The cells were incubated at 37 °C in 5% CO_2 for 72 h. Then, fresh media containing MTT (0.40 mg mL^{-1}) were added into the above 96-well plates, which were incubated at 37 °C for an additional 4 h. Thereafter, the medium was discarded, the formazan crystals formed were dissolved in DMSO, and the absorbance was recorded at 595 nm. It was observed that the cell viability remained above 95% at different concentrations of $Pe(Cbl)_4$ and $Pe(OH)_4$ nanoparticles used, whereas an increasing cytotoxicity was observed upon the addition of increasing concentrations of chlorambucil (Figure 9a).

To investigate the photoinduced release of chlorambucil within the HeLa cancer cell line and its subsequent effect on the cell viability, the cells incubated with different concentrations of $Pe(Cbl)_4$ nanoparticles were irradiated for different time intervals under visible light (≥410 nm), resulting in the release of the anticancer drug chlorambucil to induce cytotoxicity to HeLa cells, as confirmed by the MTT toxicity studies (Figure 9b,c). On the other hand, there was no significant cell death observed when the cells were irradiated either in the presence of $Pe(OH)_4$ nanoparticles or in the absence of $Pe(Cbl)_4$ nanoparticles, demonstrating that the cytotoxicity caused was only because of the released chlorambucil drug upon the photoirradiation. By comparing four equivalents of chlorambucil with one equivalent of $Pe(Cbl)_4$ nanoparticles (Figure 9a), $Pe(Cbl)_4$ nanoparticles showed much lower cytotoxicity. Significantly, upon photoirradiation, $Pe(Cbl)_4$ nanoparticles presented an enhanced cytotoxicity (Figure 9b,c) to cancer cells as compared with that of free chlorambucil, on account

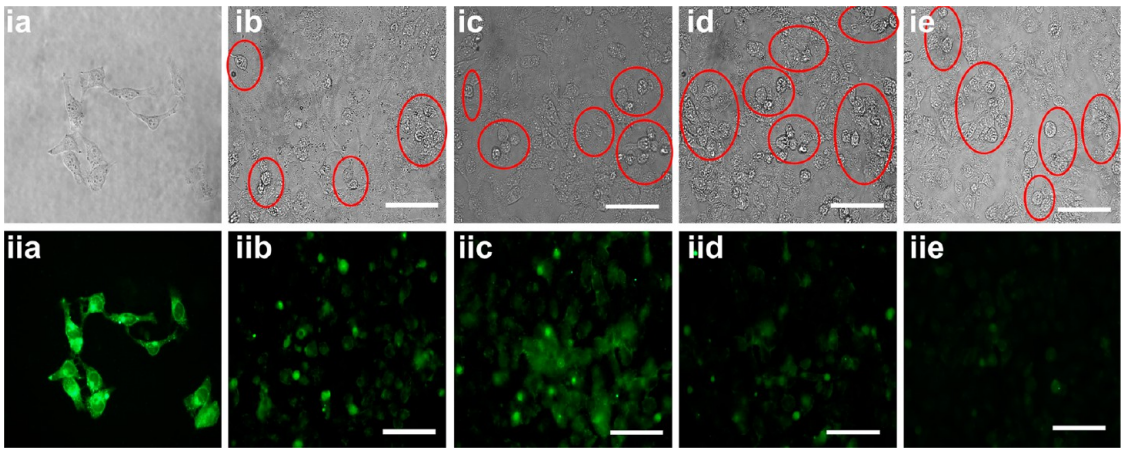

Figure 10. Confocal bright field and fluorescence images of HeLa cells incubated with Pe(Cbl)$_4$ nanoparticles (2×10^{-5} M) under different irradiation times (0−60 min, time interval = 15 min): (ia−ie) bright field and (iia−iie) corresponding fluorescence images. Red circles in (ib)−(ie) indicate the nucleus condensation of HeLa cells. Scale bar = 50 μm.

of efficient photorelease of chlorambucil within the cells.

Furthermore, cellular death caused by the released chlorambucil was confirmed by observing the changes of cell morphology and the nucleus condensation from confocal bright field images, as shown in Figure 10, ib−ie (indicated by red circles). Thus, the Pe(Cbl)$_4$ nanoparticles could be considered as a versatile DDS for photoinduced release of anticancer drug within live cells.

Real-Time Monitoring of Drug Release. To demonstrate that Pe(Cbl)$_4$ nanoparticles could serve as photoresponsive nanocarriers with real-time monitoring of the drug release, the luminescence properties of Pe(Cbl)$_4$ nanoparticles were investigated. As shown in Figure 4b, the Pe(Cbl)$_4$ nanoparticles exhibit green fluorescence with the emission maxima at 558 nm. We observed a gradual decrease in the green emission band at 558 nm for the Pe(Cbl)$_4$ nanoparticles upon increasing irradiation time. The changes in fluorescence intensity were also employed to monitor the drug release inside HeLa cells in real time using confocal fluorescence imaging technique (Figure 10). It can be clearly seen from Figure 10 that the bright green emission of Pe(Cbl)$_4$ nanoparticles in the HeLa cells observed before photoirradiation (Figure 10, iia) lost its luminescence intensity upon gradual photoirradiation and finally turned nonemissive (Figure 10, iie) after 1 h of irradiation, indicating the complete decomposition of Pe(Cbl)$_4$ nanoparticles into corresponding photoproducts Pe(OH)$_4$ and four equivalents of chlorambucil.

Tunable Emission Properties of Perylene-Derived Nanoparticles. Perylene, a polycyclic aromatic compound, is a bright blue emitting fluorophore in organic solution with the emission maxima of 440 nm. When it aggregates to form nanoparticles in aqueous solution, it shows a distinct red emission.[39] A red emissive perylene-derived organic nanoparticle based DDS, namely, PeCbl (λ_{emi} = 625 nm), was previously reported by Sing and co-workers,[40] which could release the drug under photoirradiation of visible light. The perylene-3-ylmethanol (PeOH) nanoparticles were observed to be bright blue emissive (λ_{emi} = 440 nm). The newly designed Pe(Cbl)$_4$ nanoparticles are bright green emissive (λ_{emi} = 558 nm), which is in contrast to the corresponding PRPG nanoparticles, Pe(OH)$_4$, with faint blue emission (λ_{emi} = 460 nm, Figure S9 in the SI). These four perylene derivatives were found to be bright blue emissive in organic solution (Figures S8−S15 in the SI). Thus, the perylene and perylene-derived small organic molecules show entirely distinct emission properties in solution and in the state of aggregation, and the emission properties of these aggregates could be fine-tuned by varying the substituents on the parent perylene chromophore as indicated in Figure 11.

To demonstrate the feasibility of tunable emission properties from perylene-derived nanoparticles *in vitro*, they were employed for cell imaging studies in the HeLa cancer cell line. The co-staining experiments were carried out by incubating HeLa cells with an equimolar (5 μM) mixture of PeOH, PeCbl, and Pe(Cbl)$_4$ nanoparticles for 6 h followed by recording images with a confocal microscope. The images reveal that the three types of nanoparticles were simultaneously internalized by the cells, and their corresponding emission color was retained in the cellular environment as shown in Figure 12a−d.

To better understand the tunable emission properties of perylene-derived nanoparticles, the relative energies of the frontier molecular orbitals for each nanoparticle system were investigated by measuring their oxidation/reduction potentials under cyclic voltammetry (CV), and the subsequent energy levels associated with the corresponding nanoparticles were calculated as represented in Scheme 3. The voltammograms (Figures S17−S20 in the SI) indicate that all nanoparticles undergo single irreversible oxidation.

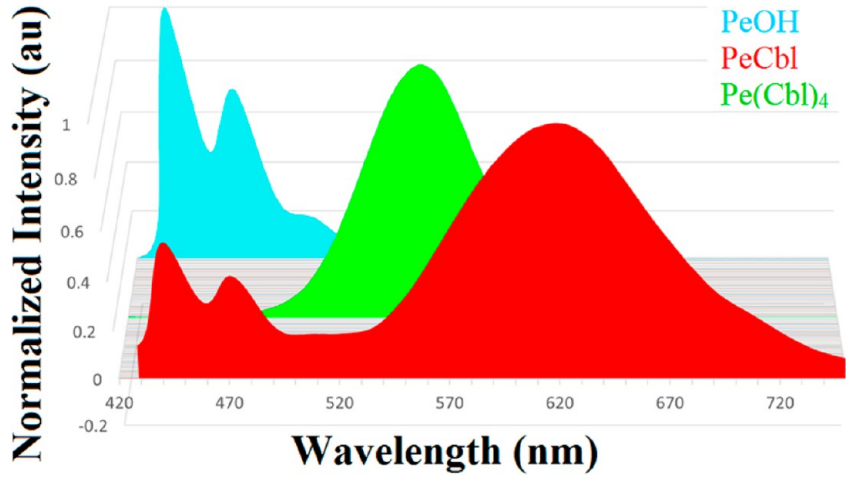

Figure 11. Normalized emission spectra of PeOH, PeCbl, and $Pe(Cbl)_4$ nanoparticles in water.

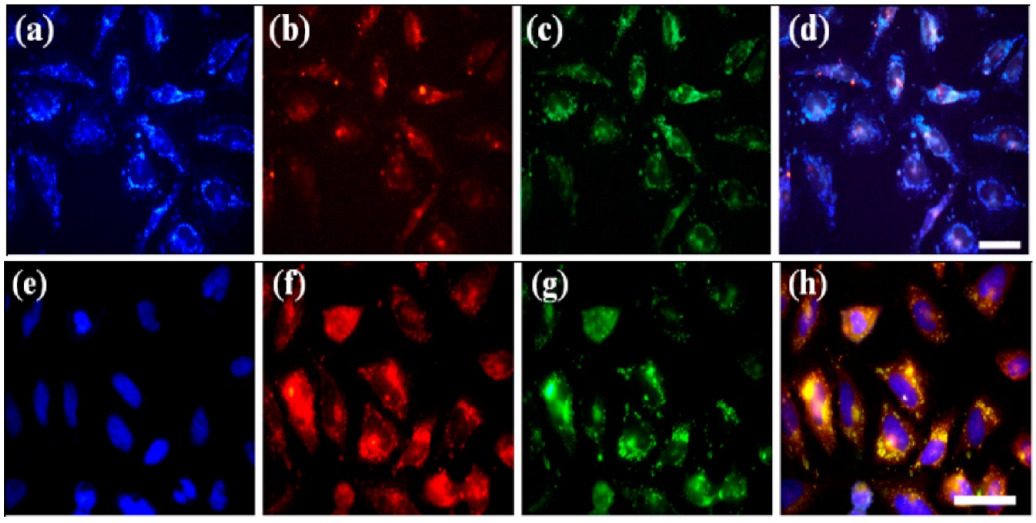

Figure 12. Co-localization studies of PeOH, PeCbl, and $Pe(Cbl)_4$ nanoparticles in HeLa cells: (a) emission from PeOH nanoparticles, (b) emission from PeCbl nanoparticles, (c) emission from $Pe(Cbl)_4$ nanoparticles, (d) overlay image of (a, b, and c) showing the co-localization of three types of nanoparticles. Scale bar = 20 μm. (e) Emission from DAPI, (f) emission from PeCbl nanoparticles, (g) emission from $Pe(Cbl)_4$ nanoparticles, (h) overlay image of (e, f, and g) demonstrating the co-localization of both PeCbl and $Pe(Cbl)_4$ nanoparticles within the cell cytoplasm (yellow color in image h). Scale bar = 50 μm.

The oxidation potential (E_{ox}) for each nanoparticle system, corresponding to the HOMO, was calculated by following the literature procedure,[41] and the band gap energy (E_{0-0}) for the corresponding nanoparticles was obtained from the intersection of the normalized absorption and emission spectra. It can be clearly seen from Scheme 3 that the PeOH nanoparticles possess the highest HOMO−LUMO energy barrier (3.06eV) followed by the $Pe(OH)_4$ nanoparticles (2.76eV), and that they emit at the higher energy blue-emitting region. The PeCbl nanoparticles have the lowest HOMO−LUMO energy barrier (2.31 eV), which falls in the lower energy red-emitting region. In the case of $Pe(Cbl)_4$ nanoparticles having an intermediate HOMO−LUMO energy barrier of 2.43eV, their emission is within the relatively high energy green-emitting region.

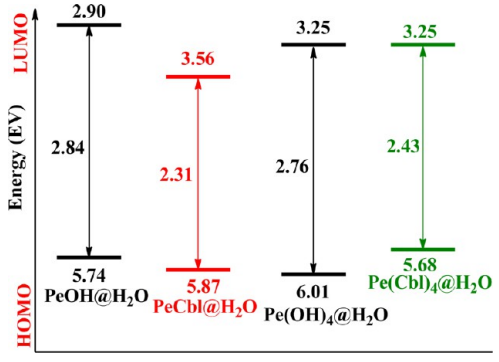

Scheme 3. Relative energies for the HOMO and LUMO levels of PeOH, $Pe(OH)_4$, PeCbl, and $Pe(Cbl)_4$ nanoparticles evaluated from respective ground-state redox potentials and E_{0-0} values.

Evaluation of *in Vivo* Toxicology of $Pe(OH)_4$ Nanoparticles. It was found that the $Pe(OH)_4$ nanoparticles could form a clear suspension in FBS even at a concentration of 500 μM. In order to validate the perylene-derived DDSs

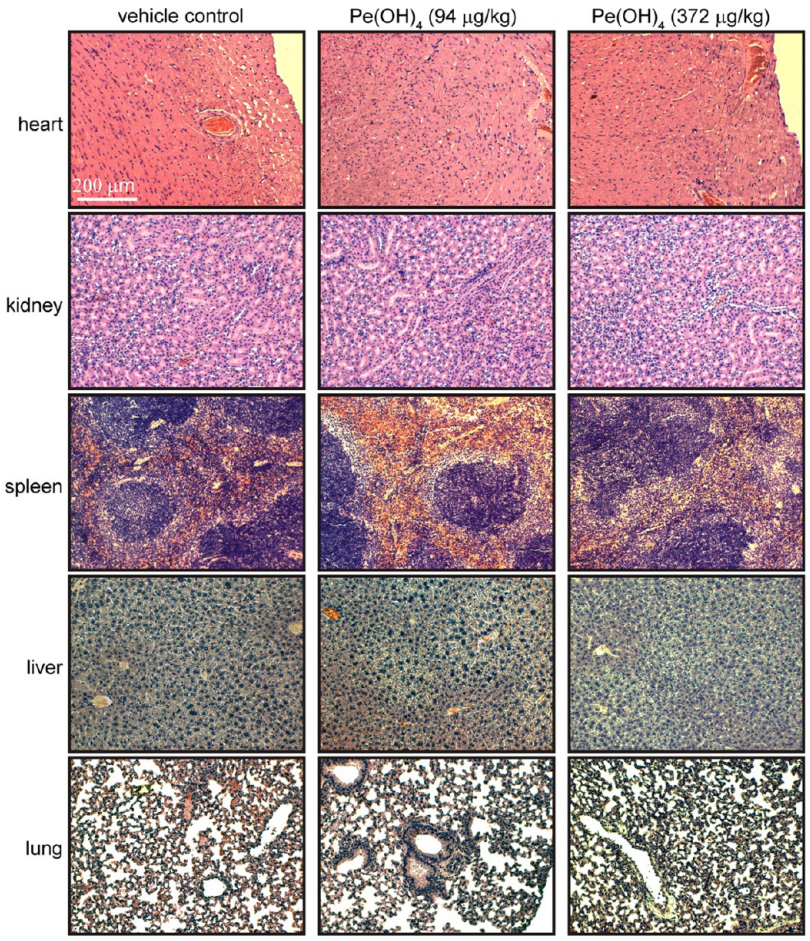

Figure 13. Representative hematoxylin and eosin stained tissue sections of the five major organs (heart, kidney, spleen, liver, and lung) isolated from the mice with and without treatment with $Pe(OH)_4$ nanoparticles, showing no obvious signs of perylene-related toxicity. Scale bar = 200 μm.

to be applicable for practical delivery of anticancer drugs, the *in vivo* toxicity of $Pe(OH)_4$ nanoparticles in the C57BL/6 mouse model was thoroughly examined. The animal studies were approved by the Institutional Animal Care and Use Committee (ARF-SBS/NIE-A0155AZ), Nanyang Technological University, and all experiments were carried out in strict compliance with the regulations. C57BL/6 mice (4−6 weeks old) were treated with $Pe(OH)_4$ nanoparticles at different concentrations (94 or 372 μg/kg) and a control of 1× PBS by intravenous injection every 3 days over a period of 4 weeks. All animals were maintained in specific pathogen-free conditions. The weight, movement, and red blood cell count of the mice were monitored daily. During the 4-week treatment with $Pe(OH)_4$ nanoparticles, no significant changes in the total body weight, animal movement, and total red blood cell count were observed for all the treated mice (data not shown) with respect to the mice used for control experiment, which indicates that all the mice could tolerate the treatment of $Pe(OH)_4$ nanoparticles without obvious signs of toxicity throughout the course of this study. After 4 weeks of treatment, the mice were sacrificed and the tissues of five major organs, *i.e.*, heart, kidney, spleen, liver, and lung, were harvested and analyzed for necrosis and cellular apoptosis by histology (hematoxylin and eosin staining), revealing no visible tissue necrosis for all five major organs (Figure 13). Thus, the *in vivo* toxicology studies clearly demonstrate that the $Pe(OH)_4$ nanoparticle based DDSs could be considered as safe drug carriers for future applications.

CONCLUSION

In summary, we have designed a perylene-derived single-component organic nanoparticle-based drug delivery system for photocontrolled intracellular delivery of an anticancer drug. The bright green emission of $Pe(Cbl)_4$ nanoparticles has been utilized for *in vitro* cellular imaging. The photoinduced drug release capability of the $Pe(Cbl)_4$ nanoparticles has been established by exposure to visible light. Photoinduced cytotoxicity enhancement of the $Pe(Cbl)_4$ nanoparticles as compared to free drug against HeLa cells has been demonstrated. Furthermore, the *in vivo* toxicology studies of $Pe(OH)_4$ nanoparticles has revealed that the perylene-derived organic nanoparticles could be considered as safe drug delivery vehicles. In addition,

we have for the first time developed organic nanoparticle systems with tunable emission properties by varying the substituents on the parent chromophore. Thus, it is possible to obtain emission in the entire spectrum by introducing suitable substituents at suitable positions on the parent perylene unit in the future. The present findings may open up a new area of designing multicolor-emitting organic nanoparticles for different applications such as bioimaging, bioanalytics, and optoelectronics.

MATERIALS AND METHODS

General Information. All reagents were purchased from Sigma-Aldrich and used without further purification. Acetonitrile and dichloromethane were distilled from CaH_2 before use. ^1H NMR spectra were recorded on a Bruker-AC 300 MHz spectrometer. Chemical shifts are reported in ppm from tetramethylsilane with the solvent resonance as the internal standard (deuterochloroform: 7.26 ppm). Data are reported as follows: chemical shifts, multiplicity (s = singlet, d = doublet, t = triplet, m = multiplet), and coupling constant (Hz). ^{13}C NMR (75 MHz) spectra were recorded on a Bruker-AC 300 MHz spectrometer with complete proton decoupling. Chemical shifts are reported in ppm from tetramethylsilane with the solvent resonance as the internal standard (deuterochloroform: 77.0 ppm). UV/vis absorption spectra were recorded on a Shimadzu UV-3600 UV−vis−NIR spectrophotometer. Fluorescence emission spectra were recorded on a Shimadzu RF-5301 PC spectrofluorophotometer. FT-IR spectra were recorded on a PerkinElmer RXI spectrometer, and HRMS spectra were recorded on a JEOL-AccuTOF JMS-T100L mass spectrometer. Transmission electron microscopy images were measured on a JEM-1400 (JEOL) operated at 100−120 kV. The TEM samples were prepared by dispersing compounds in water, which were dropped on the surface of a copper grid. Scanning electron microscopy images were collected on a field emission JSM-6700F (JEOL) operated at 10 kV. Photolysis of all the ester conjugates was carried out using a 125 W (110 mW/cm^2) medium-pressure Hg lamp supplied by SAIC (India). Chromatographic purification was performed with 60−120 mesh silica gel (Merck). For monitoring reactions, precoated silica gel 60 F254 TLC sheets (Merck) were used.

Preparation of Perylene-3,4,9,10-tetracarboxylic Acid (2).[32] Perylene-3,4,9,10-tetracarboxylic dianhydride (5.0 g, 12.7 mmol) was suspended in water (100 mL) followed by the addition of potassium hydroxide (5.0 g, 89.1 mmol). The reaction mixture was heated to reflux with vigorous stirring. After 24 h, the reaction mixture was cooled to room temperature followed by acidification with 10% sulfuric acid (100 mL) to result in the precipitation. Product perylene-3,4,9,10-tetracarboxylic acid (**2**) was collected by filtration, washed with water and ethanol, and dried under vacuum. Compound **2** (5.4 g, 99%) as a dark red solid was used without further purification.

Preparation of Tetrabenzyl Perylene-3,4,9,10-tetracarboxylate (3) (ref 32). A solution containing compound **2** (2.5 g, 5.8 mmol), benzyl chloride (22.2 g, 175.0 mmol), potassium carbonate (8.1 g, 58.4 mmol), 18-crown-6 (1.5 g, 5.8 mmol), and 4-(dimethylamino)pyridine (0.7 g, 5.8 mmol) in DMF (50 mL) was heated at 90 °C with stirring under a nitrogen atmosphere. After 24 h, the reaction mixture was cooled to room temperature and was then filtered under suction and washed with DMF (20 mL) to remove insoluble materials and excess potassium carbonate. The solvent was removed using a rotary evaporator under reduced pressure. The residue obtained after the removal of the solvent was washed with 50% aqueous ethanol (50 mL) and dried under vacuum to give tetrabenzyl perylene-3,4,9,10-tetracarboxylate, **3** (3.7 g, 86%), as an orange solid. The compound was further purified by flash chromatography using dichloromethane as the mobile phase to yield orange crystals of **3**. ^1H NMR ($CDCl_3$, 300 MHz): δ 5.16 (s, 8H), 7.32−7.36 (m, 24H), 7.99 (d, J = 7.9 Hz, 4H).

Preparation of Perylene-3,4,9,10-tetrayltetramethanol (4) (ref 32). To a solution of compound **3** (4.5 g, 5.7 mmol) in dichloromethane (50 mL) was dropwise added a solution of diisobutylaluminum hydride (DIBALH, 1.0 M in THF, 28.5 mL, 28.5 mmol) at −78 °C. After 30 min at this temperature, the reaction mixture was warmed to room temperature, stirred for an additional 48 h, and quenched by slow addition of ethanol (25 mL). Then, the solvent was evaporated under vacuum to obtain a bright orange glassy solid. After complete drying under vacuum, the residue was protonated by treatment with 10% sulfuric acid (60 mL), affording red powders. The resultant powders were collected by filtration, washed with water (60 mL) and ethanol (13 mL), and then dried under vacuum to give perylene-3,4,9,10-tetrayltetramethanol (2.0 g, 92%). ^1H NMR (DMSO-d_6, 300 MHz): δ 5.07 (s, 8H), 5.32 (bs, 4H, OH), 7.68−7.70 (d, J = 7.8 Hz, 4H), 8.34−8.37 (d, J = 7.8 Hz, 4H).

Synthesis of Pe(Cbl)$_4$ Conjugate. A mixture of chlorambucil (0.4 g, 1.3 mmol), EDCL (0.3 g, 1.3 mmol), and DMAP (0.1 g, 1.1 mmol) was dissolved in dry dichloromethane, and the reaction mixture was vigorously stirred under a nitrogen atmosphere at room temperature for 1 h. Then, the compound $Pe(OH)_4$ (0.1 g, 0.3 mmol) was added followed by the addition of DMAP (0.1 g, 1.1 mmol). The reaction mixture was stirred under dark conditions at room temperature overnight. After completion of the reaction, the resulting product was extracted in dichloromethane from a dichloromethane/H_2O mixture. The organic fraction was dried over anhydrous Na_2SO_4 followed by the removal of solvent under reduced pressure to yield a brown residue, which was further purified by flash column chromatography using 30% ethyl acetate in hexane as the mobile phase to afford compound **6** as a yellow solid (0.2 g, 79%). ^1H NMR ($CDCl_3$, 300 MHz): δ 1.86−1.96 (m, 8H), 2.38 (t, J = 14.7 Hz, 8H), 2.51 (t, J = 15.0 Hz, 8H), 3.55−3.68 (m, 32H), 5.64 (s, 8H), 6.53−6.56 (d, J = 8.7 Hz, 8H), 6.95−6.98 (d, J = 8.4 Hz, 8H), 7.71−7.74 (d, J = 7.8 Hz, 4H), 8.22−8.25 (d, J = 7.8 Hz, 4H). ^{13}C NMR ($CDCl_3$, 75 Hz): δ 26.6, 33.7, 33.9, 40.5, 53.6, 66.7, 112.1, 121.3, 129.7, 129.9, 130.4, 131.3, 132.4, 132.6, 132.9, 144.3, 173.1. IR (KBR): 1725 cm^{-1}. HRMS: calculated for $C_{80}H_{88}Cl_8N_4O_8Na$ $[M + Na]^+$ 1535.4008, mass obtained 1535.4031.

Preparation of Pe(Cbl)$_4$ Nanoparticles. The $Pe(Cbl)_4$ nanoparticles were synthesized by following the reprecipitation technique as described in a previous report.[2] Basically, $Pe(Cbl)_4$ conjugate in acetone (10 μL, 5 mM) was slowly added into water (5 mL) at room temperature with constant sonication for 30 min. The size of the $Pe(Cbl)_4$ nanoparticles was determined by TEM as well as DLS.

Preparation of Pe(OH)$_4$ Nanoparticles. Synthesis of $Pe(OH)_4$ nanoparticles was carried out by following the same procedure as described in the case of $Pe(Cbl)_4$ nanoparticles.

Hydrolytic Stability of Pe(Cbl)$_4$ Nanoparticles at Different pH. A suspension (1 mL, 2×10^{-4} M) of $Pe(Cbl)_4$ nanoparticles was added into a PBS solution (1 mL) under different pH. The PBS culture medium contained 10% FBS with pH = 7.4. All the tubes were kept in an ultrasonic bath for 10 min to make the suspensions homogeneous, which were stored at 37 °C in dark conditions for 72 h. Then, the organic compounds were extracted in dichloromethane and the ^1H NMR spectra were recorded to examine the remaining percentage of the $Pe(Cbl)_4$ conjugate.

Photolysis of Pe(Cbl)$_4$ Nanoparticles under Visible Light Irradiation. An aqueous suspension (100 mL, 1×10^{-4} M) of the $Pe(Cbl)_4$ nanoparticles was prepared. Half of the suspension was kept in the dark. The other half was irradiated using a 125 W (110 mW/cm^2) medium-pressure Hg lamp as the light source (≥410 nm) with a solution filter of $NaNO_2$ solution (1 M) under a nitrogen atmosphere. At a regular interval of time, a certain amount (5 mL) of solution was taken, which was extracted in dichloromethane. The percentage of $Pe(Cb)_4$ decomposed was

quantified by ^{1}H MNR spectra. From the ^{1}H NMR spectra, it was observed that, upon photoirradiation, the $Pe(Cbl)_4$ conjugate underwent photocleavage of the ester C−O bond at 5.64 ppm to produce the corresponding photoproducts along with chlorambucil.

$Pe(Cbl)_4$ Nanoparticles for Cell Imaging on the HeLa Cell Line. Cell imaging studies were carried out using the HeLa cell line, which was maintained in minimum essential medium (MEM) containing 10% FBS at 37 °C and 5% CO_2. To study the cellular uptake of $Pe(Cbl)_4$ nanoparticles, HeLa cells (5×10^4 cells/well) were placed on six-well plates and allowed to adhere for 4−8 h. The cells were then incubated with $Pe(Cbl)_4$ nanoparticles (5×10^{-6} M) in cell culture medium at 37 °C and 5% CO_2 for 6 h. Thereafter, the cells were fixed in 4% aqueous formaldehyde for 15 min and washed two times with PBS. Imaging was captured by a Nikon confocal microscope (Nikon Eclipse TE2000-E) using the respective filter.

Intracellular Trafficking of $Pe(Cbl)_4$ Nanoparticles. Cells, grown and plated as described above, were incubated with MEM (1 mL) containing $Pe(Cbl)_4$ nanoparticles (5×10^{-6} M) at 37 °C for 6 h. Thereafter, the cells were washed two times with PBS (10 mM) and fixed with 4% aqueous formaldehyde at room temperature for 15 min. After fixation, the cells were washed three times with PBS (10 mM). The cells were counterstained with DAPI (0.3 μM) at room temperature in the dark for 5 min. After gentle washing in PBS (10 mM) two times, the cells were viewed under a confocal microscope.

Lyso Tracking Experiment. To study the intracellular localization of $Pe(Cbl)_4$ nanoparticles, HeLa cells (5×10^4 cells/well) were placed on a coverslip in a six-well cell culture plate and allowed to adhere for 8 h. The cells were then incubated with $Pe(Cbl)_4$ nanoparticles (5×10^{-5} M) in PBS at 37 °C and 5% CO_2 for 6 h. Then, the medium was discarded, and the cells were washed two times with PBS. LysoTracker Red DND-99 (2 mL, 50 nM) in DMEM culture medium was added into the cells, which were incubated at 37 °C and 5% CO_2 for 1 h. Thereafter, the cells were fixed in 4% formaldehyde for 15 min and washed two times with PBS. Imaging was captured by a Nikon confocal microscope using the respective filter.

Cytotoxicity before Photolysis. The cytotoxicity *in vitro* was measured using the MTT assay on the HeLa cell line. Briefly, cells growing in log phase were seeded into a 96-well cell culture plate at 1×10^4 cells/mL. $Pe(Cbl)_4$ nanoparticles, $Pe(OH)_4$ nanoparticles, and chlorambucil were added into the wells with an equal volume of PBS in the control wells. The cells were then incubated at 37 °C in 5% CO_2 for 72 h. Thereafter, fresh media containing MTT (0.40 mg mL^{-1}) were added to the 96-well plate and incubated at 37 °C in 5% CO_2 for an additional 4 h. Formazan crystals formed were dissolved in DMSO after decanting the media, and then absorbance was recorded at 595 nm.

Cytotoxicity after Photolysis. HeLa cells in a 96-well cell culture plate at a concentration of 1×10^4 cells/mL were maintained in MEM containing 10% FBS. $Pe(Cbl)_4$ nanoparticles (0.01−10 μM), $Pe(OH)_4$ nanoparticles (0.01−10 μM), and chlorambucil (0.04−40 μM) with different concentrations were incubated at 37 °C and 5% CO_2 for 6 h. Then, the cells were irradiated using a 125 W (110 mW/cm^2) medium-pressure Hg lamp as the irradiation source (≥410 nm) with $NaNO_2$ solution (1 M) as a UV cutoff filter by keeping the cell culture plate 5 cm away from the light source. After irradiation, the cells were incubated for another 72 h. Finally, the cytotoxicity was measured using the MTT assay as described in the previous section.

Conflict of Interest: The authors declare no competing financial interest.

Supporting Information Available: Synthetic details and characterization data. This material is available free of charge *via* the Internet at http://pubs.acs.org.

Acknowledgment. A.J., N.K.T., and Y.Z. thank the National Research Foundation (NRF), Prime Minister's Office, Singapore, under its NRF Fellowship (NRF2009NRF-RF001-015) and Campus for Research Excellence and Technological Enterprise (CREATE) programme-Singapore Peking University Research Centre for a Sustainable Low-Carbon Future, the NTU-A*Star Centre of Excellence for Silicon Technologies (A*Star SERC No. 112 351 0003), for financial support. X.L. acknowledges a grant from the Carl Tryggers Foundation and computational resources provided by the Swedish National Infrastructure for Computing for the project "Multiphysics Modeling of Molecular Materials", SNIC 025/12-38.

REFERENCES AND NOTES

1. Peer, D.; Karp, J. M.; Hong, S.; Farokhzad, O. C.; Margalit, R.; Langer, R. Nanocarriers as an Emerging Platform for Cancer Therapy. *Nat. Nanotechnol.* **2007**, *2*, 751–760.
2. Dreaden, E. C.; Gryder, B. E.; Austin, L. A.; Tene Defo, B. A.; Hayden, S. C.; Pi, M.; Quarles, L. D.; Oyelere, A. K.; El-Sayed, M. A. Antiandrogen Gold Nanoparticles Dual-Target and Overcome Treatment Resistance in Hormone-Insensitive Prostate Cancer Cells. *Bioconjugate Chem.* **2012**, *23*, 1507–1512.
3. Lee, S.-M.; Kim, H. J.; Ha, Y.-J.; Park, Y. N.; Lee, S.-K.; Park, Y.-B.; Yoo, K.-H. Targeted Chemo-Photothermal Treatments of Rheumatoid Arthritis Using Gold Half-Shell Multifunctional Nanoparticles. *ACS Nano* **2013**, *7*, 50–57.
4. Nowicka, A. M.; Kowalczyk, A.; Jarzebinska, A.; Donten, M.; Krysinski, P.; Stojek, Z.; Augustin, E.; Mazerska, Z. Progress in Targeting Tumor Cells by Using Drug-Magnetic Nanoparticles Conjugate. *Biomacromolecules* **2013**, *14*, 828–833.
5. Wang, C.; Xu, H.; Liang, C.; Liu, Y.; Li, Z.; Yang, G.; Cheng, L.; Li, Y.; Liu, Z. Iron Oxide@Polypyrrole Nanoparticles as a Multifunctional Drug Carrier for Remotely Controlled Cancer Therapy with Synergistic Antitumor Effect. *ACS Nano* **2013**, *7*, 6782–6795.
6. Wang, F.; Wang, Y.-C.; Dou, S.; Xiong, M.-H.; Sun, T.-M.; Wang, J. Doxorubicin-Tethered Responsive Gold Nanoparticles Facilitate Intracellular Drug Delivery for Overcoming Multidrug Resistance in Cancer Cells. *ACS Nano* **2011**, *5*, 3679–3692.
7. Argyo, C.; Weiss, V.; Bräuchle, C.; Bein, T. Multifunctional Mesoporous Silica Nanoparticles as a Universal Platform for Drug Delivery. *Chem. Mater.* **2014**, *26*, 435–451.
8. Lai, J.; Shah, B. P.; Garfunkel, E.; Lee, K.-B. Versatile Fluorescence Resonance Energy Transfer-Based Mesoporous Silica Nanoparticles for Real-Time Monitoring of Drug Release. *ACS Nano* **2013**, *7*, 2741–2750.
9. Lee, J. E.; Lee, N.; Kim, T.; Kim, J.; Hyeon, T. Multifunctional Mesoporous Silica Nanocomposite Nanoparticles for Theranostic Applications. *Acc. Chem. Res.* **2011**, *44*, 893–902.
10. Mackowiak, S. A.; Schmidt, A.; Weiss, V.; Argyo, C.; Von Schirnding, C.; Bein, T.; Bräuchle, C. Targeted Drug Delivery in Cancer Cells with Red-Light Photoactivated Mesoporous Silica Nanoparticles. *Nano Lett.* **2013**, *13*, 2576–2583.
11. Zhao, Y.; Lin, L.-N.; Lu, Y.; Chen, S.-F.; Dong, L.; Yu, S.-H. Templating Synthesis of Preloaded Doxorubicin in Hollow Mesoporous Silica Nanospheres for Biomedical Applications. *Adv. Mater.* **2010**, *22*, 5255–5259.
12. DeCock, L. J.; DeKoker, S.; DeGeest, B. G.; Grooten, J.; Vervaet, C.; Remon, J. P.; Sukhorukov, G. B.; Antipina, M. N. Polymeric Multilayer Capsules in Drug Delivery. *Angew. Chem., Int. Ed.* **2010**, *49*, 6954–6973.
13. Ahmed, F.; Pakunlu, R. I.; Srinivas, G.; Brannan, A.; Bates, F.; Klein, M. L.; Minko, T.; Discher, D. E. Shrinkage of a Rapidly Growing Tumor by Drug-Loaded Polymersomes: pH-Triggered Release Through Copolymer Degradation. *Mol. Pharmaceut.* **2006**, *3*, 340–350.
14. Gingras, M.; Roy, M. In *Dendrimer-Based Drug Delivery Systems*; John Wiley & Sons, Inc.: New York, 2012; p 239.
15. Gillies, E. R.; Fréchet, J. M. J. Dendrimers and Dendritic Polymers in Drug Delivery. *Drug Discovery Today* **2005**, *10*, 35–43.
16. Choi, S. K.; Verma, M.; Silpe, J.; Moody, R. E.; Tang, K.; Hanson, J. J.; Baker, J. R., Jr. A Photochemical Approach for Controlled Drug Release in Targeted Drug Delivery. *Bioorg. Med. Chem.* **2012**, *20*, 1281–1290.
17. Antimisiaris, S. G.; Kallinteri, P.; Fatouros, D. G. In *Pharmaceutical Manufacturing Handbook*; John Wiley & Sons, Inc.: New York, 2007; p 443.

18. Gabizon, A. A. Pegylated Liposomal Doxorubicin: Metamorphosis of an Old Drug into a New Form of Chemotherapy. *Cancer Invest.* **2001**, *19*, 424–436.
19. Barenholz, Y. Doxil-The First FDA-Approved Nano-Drug: Lessons Learned. *J. Controlled Release* **2012**, *160*, 117–134.
20. Biswas, S.; Vaze, O. S.; Movassaghian, S.; Torchilin, V. P. In *Drug Delivery Strategies for Poorly Water-Soluble Drugs*; John Wiley & Sons Ltd: New York, 2013; p 411.
21. Lee, E. S.; Na, K.; Bae, Y. H. Doxorubicin Loaded pH-Sensitive Polymeric Micelles for Reversal of Resistant MCF-7 Tumor. *J. Controlled Release* **2005**, *103*, 405–418.
22. Singh, N.; Karambelkar, A.; Gu, L.; Lin, K.; Miller, J. S.; Chen, C. S.; Sailor, M. J.; Bhatia, S. N. Bioresponsive Mesoporous Silica Nanoparticles for Triggered Drug Release. *J. Am. Chem. Soc.* **2011**, *133*, 19582–19585.
23. Schloßbauer, A.; Sauer, A. M.; Cauda, V.; Schmidt, A.; Engelke, H.; Rothbauer, U.; Zolghadr, K.; Leonhardt, H.; Bräuchle, C.; Bein, T. Cascaded Photoinduced Drug Delivery to Cells from Multifunctional Core-Shell Mesoporous Silica. *Adv. Healthcare Mater.* **2012**, *1*, 316–320.
24. Fan, N.-C.; Cheng, F.-Y.; Ho, J.-a. A.; Yeh, C.-S. Photocontrolled Targeted Drug Delivery: Photocaged Biologically Active Folic Acid as a Light-Responsive Tumor-Targeting Molecule. *Angew. Chem., Int. Ed.* **2012**, *51*, 8806–8810.
25. Frasconi, M.; Liu, Z.; Lei, J.; Wu, Y.; Strekalova, E.; Malin, D.; Ambrogio, M. W.; Chen, X.; Botros, Y. Y.; Cryns, V. L.; *et al.* Photoexpulsion of Surface-Grafted Ruthenium Complexes and Subsequent Release of Cytotoxic Cargos to Cancer Cells from Mesoporous Silica Nanoparticles. *J. Am. Chem. Soc.* **2013**, *135*, 11603–11613.
26. Vivero-Escoto, J. L.; Slowing, I. I.; Wu, C.-W.; Lin, V. S. Y. Photoinduced Intracellular Controlled Release Drug Delivery in Human Cells by Gold-Capped Mesoporous Silica Nanosphere. *J. Am. Chem. Soc.* **2009**, *131*, 3462–3463.
27. Ge, J.; Neofytou, E.; Cahill, T. J.; Beygui, R. E.; Zare, R. N. Drug Release from Electric-Field-Responsive Nanoparticles. *ACS Nano* **2011**, *6*, 227–233.
28. Yan, H.; Teh, C.; Sreejith, S.; Zhu, L.; Kwok, A.; Fang, W.; Ma, X.; Nguyen, K. T.; Korzh, V.; Zhao, Y. Functional Mesoporous Silica Nanoparticles for Photothermal-Controlled Drug Delivery in Vivo. *Angew. Chem., Int. Ed.* **2012**, *51*, 8373–8377.
29. Mayer, G.; Heckel, A. Biologically Active Molecules with a "Light Switch". *Angew. Chem., Int. Ed.* **2006**, *45*, 4900–4921.
30. Ellis-Davies, G. C. R. Caged Compounds: Photorelease Technology for Control of Cellular Chemistry and Physiology. *Nat. Meth.* **2007**, *4*, 619–628.
31. Lee, H.-M.; Larson, D. R.; Lawrence, D. S. Illuminating the Chemistry of Life: Design, Synthesis, and Applications of "Caged" and Related Photoresponsive Compounds. *ACS Chem. Biol.* **2009**, *4*, 409–427.
32. Takahashi, M.; Suzuki, Y.; Ichihashi, Y.; Yamashita, M.; Kawai, H. 1,3,8,10-Tetrahydro-2,9-Diazadibenzo[cd,lm]perylenes. Synthesis of Reduced Perylene Bisimide Analogues. *Tetrahedron Lett.* **2007**, *48*, 357–359.
33. Seko, T.; Ogura, K.; Kawakami, Y.; Sugino, H.; Toyotama, H.; Tanaka, J. Excimer Emission of Anthracene, Perylene, Coronene and Pyrene Microcrystals Dispersed in Water. *Chem. Phys. Lett.* **1998**, *291*, 438–444.
34. Jana, A.; Ikbal, M.; Singh, N. D. P. Perylen-3-ylmethyl: Fluorescent Photoremovable Protecting Group (FPRPG) for Carboxylic Acids and Alcohols. *Tetrahedron* **2012**, *68*, 1128–1136.
35. Schade, B.; Hagen, V.; Schmidt, R.; Herbrich, R.; Krause, E.; Eckardt, T.; Bendig, J. Deactivation Behavior and Excited-State Properties of (Coumarin-4-yl)methyl Derivatives. 1. Photocleavage of (7-Methoxycoumarin-4-yl)methyl-Caged Acids with Fluorescence Enhancement. *J. Org. Chem.* **1999**, *64*, 9109–9117.
36. Becke, A. D. Density-Functional Thermochemistry. III. The Role of Exact Exchange. *J. Chem. Phys.* **1993**, *98*, 5648–5652.
37. Stephens, P. J.; Devlin, F. J.; Chabalowski, C. F.; Frisch, M. J. Ab Initio Calculation of Vibrational Absorption and Circular Dichroism Spectra Using Density Functional Force Fields. *J. Phys. Chem.* **1994**, *98*, 1123–11627.
38. Neese, F. Wiley Interdisciplinary Reviews. *Comput. Mol. Sci.* **2012**, *2*, 73.
39. Baba, K.; Kasai, H.; Masuhara, A.; Oikawa, H.; Nakanishi, H. Organic Solvent-Free Fluorescence Confocal Imaging of Living Cells Using Pure Nanocrystal Forms of Fluorescent Dyes. *Jpn. J. Appl. Phys.* **2009**, *48*, 117002/1–117002/4.
40. Jana, A.; Devi, K. S. P.; Maiti, T. K.; Singh, N. D. P. Perylene-3-ylmethanol: Fluorescent Organic Nanoparticles as a Single-Component Photoresponsive Nanocarrier with Real-Time Monitoring of Anticancer Drug Release. *J. Am. Chem. Soc.* **2012**, *134*, 7656–7659.
41. Pommerehne, J.; Vestweber, H.; Guss, W.; Mahrt, R. F.; Bässler, H.; Porsch, M.; Daub, J. Efficient Two Layer LEDs on a Polymer Blend Basis. *Adv. Mater.* **1995**, *7*, 551–554.